

Variational Inference Background Subtraction Algorithm for in-Camera Acceleration in Thermal Imagery

Konstantinos Makantasis, Antonis Nikitakis, Anastasios Doulamis, Nikolaos Doulamis, and Yannis Papaefstathiou

Abstract—Detection of moving objects in videos is a crucial step towards successful surveillance and monitoring applications. A key component for such tasks is usually called background subtraction and tries to extract regions of interest from the image background for further processing or action. For this reason, its accuracy and its real-time performance is of great significance. Although, effective background subtraction methods have been proposed, only a few of them take into consideration the special characteristics of thermal imagery. In this work, we propose a novel background subtraction scheme, which models the thermal responses of each pixel as a mixture of Gaussians with unknown number of components. Following a Bayesian approach, our method automatically estimates the mixture structure, while simultaneously it avoids over/under fitting. The pixel density estimate is followed by an efficient and highly accurate updating mechanism, which permits our system to be automatically adapted to dynamically changing operation conditions. We propose a reference implementation of our Background Subtraction Parallel System in Reconfigurable Hardware achieving both adequate performance and low power consumption. By adopting a High Level Synthesis design flow we were able to map demanding floating point arithmetic operations of our scheme in reconfigurable hardware; demonstrating fast-prototyping and on-field customization at the same time.

Index Terms—Thermal imaging, variational inference, background subtraction, foreground estimation.

I. INTRODUCTION

HIGH level computer vision applications, ranging from video surveillance and monitoring to intelligent vehicles, utilize information that corresponds to visible spectrum. However, under certain environmental conditions, this type of sensing can be severely impaired, which emerges the necessity for imaging beyond the visible spectrum, exploiting thermal sensors. Pixel values of thermal images correspond to the relative differences in the amount of thermal energy emitted or reflected from objects in the scene. Due to this fact thermal cameras are equally applicable both for day and night scenarios, while at the same time are less affected by illumination changes. Furthermore, thermal imagery eliminates any privacy issues as people being depicted can not be identified [1].

K. Makantasis is with the School of Production Engineering and Management, Technical University of Crete, Chania, 73100 Greece e-mail: kmakantasis@isc.tuc.gr

A. Nikitakis and Y. Papaefstathiou are with the School of Electrical and Computer Engineering, Technical University of Crete, Chania, 73100 Greece e-mail: a.s.nikitakis@gmail.com, ygp@mhl.tuc.gr

A. Doulamis and N. Doulamis are with the School of Rural and Surveying Engineering, National Technical University of Athens, Athens, 15780 Greece e-mail: adoulam@cs.ntua.gr, ndoulam@cs.ntua.gr

However, thermal sensors present their own unique challenges. First, they have low signal-to-noise ratio implying the existence of noisy data. Second, there is a lack of color and texture information deteriorating visual content interpretation [2]. Third, objects are not thermally homogeneous and they are exposed to variations of sun illumination adding more complexity [3], [4]. All these issues complicate pixel modeling especially when applying for object categorization and foreground/background detection.

For many high level vision-based applications, either they use visual-optical videos [5], [6], [7], [8] or thermal data [9], [10], [2], the task of background subtraction constitutes a key component for locating moving objects. The most common approach to model the background is to use mixtures of Gaussian components, the number of which are assumed to be a priori known. While such assumption is valid for sensors capturing the visible spectrum, mainly due to their ultra high resolution accuracy, that is, high signal-to-noise ratio, they are inappropriate for thermal data. Selection of a large number of components results in modeling the noise and therefore it reduces discrimination performance. On the contrary, low number of Gaussian components yield approximate modeling that fails to capture the complexity of a scene. Consequently, methods that automatically estimate the most suitable Gaussian components to fit the current statistics of thermal data are important towards an efficient background subtraction scheme.

Towards this direction, Variational Inference (VI) has been recently proposed in statistics [11] to overcome the assumption of a fixed a priori known number of Gaussian components under a computationally efficient framework in contrast to brute force techniques that build several models of different number of components to select the best ones. In addition, to increase the penetration degree of thermal sensors to the surveillance market, embedded (in-camera) acceleration methods are needed. This means that the background subtraction algorithms, exploiting Variational Inference, should be properly re-designed to be implemented in devices of low-power and memory requirements. This way, the benefits are twofold. First, we offload a significant computation load near the source of the data (i.e., camera sensor) and thus bandwidth is saved as only the region of interest (or just a triggered event) is transmitted. Second, costly operations are executed in low-power embedded hardware saving valuable resources.

A. Related Work

Background subtraction techniques applied on visual-optical videos model the color properties of depicted objects [12], [13] and can be classified into three main categories [14]: *basic background modeling* [15], [16], *statistical background modeling* [17], [18] and *background estimation* [19], [20]. The most used methods are the statistical ones due to their robustness to critical application scenarios.

In order to statistically represent the background, a probability distribution is used to model the history of pixel intensities over time. Towards this direction, the work of Stauffer and Grimson [21], is one of the best known approaches. It uses a Gaussian Mixture Model (GMM), with a fixed number of components, for a per-pixel density estimate. Similar to this approach, the work of [22] proposes a Student-t mixture model improving compactness and robustness to noise and outliers. The works of [23] and [24] extend the method of [21] by introducing a user defined threshold to estimate the number of components. However, this rule is application dependent and not directly derived from the data statistics.

Haines and Xiang in [25] address this drawback by using a Dirichlet Process Mixture Model (DPMM). This method automatically estimates the number of components by utilising sampling techniques. However, sampling algorithms are computational and memory inefficient and thus inappropriate for real-time applications. To address this problem, the authors propose a GPU implementation. All of the aforementioned techniques present the drawback that objects' color properties are highly affected by scene illumination conditions, making the same object to look completely different under different lighting or weather conditions.

Although, thermal imagery can provide a challenging alternative for addressing the aforementioned difficulty, there exist few works for thermal data. The authors of [26], [3], [27] exploit contour saliency to extract foreground objects by utilizing a unimodal background modeling technique to detect regions of interest. However, unimodal background modeling is not usually capable of capturing the background dynamics and its complexity. Baf *et al.* in [14] present a fuzzy statistical method for background subtraction to incorporate uncertainty into the mixture of Gaussians. Elguebaly and Bouguila in [28] propose a finite asymmetric generalized Gaussian mixture model for object detection. However, both of these methods require a predefined maximum number of components, presenting therefore limitations when they are applied on uncontrolled environments. Dai *et al.* in [29] propose a method for pedestrian detection and tracking using thermal imagery. This method consists of a background subtraction technique that exploits a two-layer representation (one for foreground and one for background) of frame sequences. However, the assumption made is that the foreground is restricted to moving objects, a consideration which is not sufficient for dynamically changing environments. One way to handle the aforementioned difficulties is to introduce a background model, the parameters and the structure of which are directly estimated from the data, while at the same time it takes into account the specific characteristics of thermal imagery.

The computational cost and thus the performance of a subtraction algorithm is always an issue as they usually perform poor in regular CPUs. One of the first attempts for real-time performance using a Gaussian segmentation was the work of [18] implemented in SGI O2 computer. After the introduction of [18], many implementations in hardware and GPU were presented. For example, [30] and [31] present an implementation based on the model of [21] achieving real-time performance even for High-Definition (HD) resolutions. In the work of [32] the authors managed to accelerate the algorithm of [23] up to 1080p resolution of 60fps. However, GPUs cannot be considered low power devices which can be seen as a disadvantage especially for 24/7 surveillance systems.

This gap is addressed from Field Programmable Gate Arrays (FPGA) accelerators. In the work of [33] and the later improvement of [34] the authors propose a real-time video segmentation/surveillance system using a GMM also handling memory bandwidth reduction requirements. Other approaches such as the work of [35] propose accelerators of the GMM algorithm in reconfigurable hardware reaching 24frames per second (fps) for HD video. The same authors claim even better performance of 91fps in HD video in their improved work of [36] if a Xilinx Virtex 4 device is used. However, the main limitation to achieve this performance is the memory bandwidth which becomes the main bottleneck in the pipeline. The requested bandwidth for this performance is about 8GB/sec where FPGA boards usually hold 64bit-wide Dynamic Random Access Memory (DRAM) clocked in a range of 100-200 MHz. As a result the memory subsystem can support at least one order of magnitude lower bandwidth. This means that we need technologies for reducing memory requirements in case that the background subtraction algorithm is adapted to be implemented under reconfigurable hardware architectures. Furthermore, most FPGA approaches are based on a VHDL design flow, which requires long development and testing times and also may pose restrictions in parametrization of the algorithm.

B. Our Contribution

This work presents a background modeling method able to provide a per pixel density estimate, taking into account the specific characteristics of thermal imagery. Our method exploits a GMM with unknown number of components, which are dynamically estimated directly from the data to fit their current statistical characteristics. The advantage of this approach is that it allows effective background modeling under uncontrolled and changing environments.

The VI framework is adopted to associate the functional structure of the model with real data distributions obtained from thermal images. In particular, the adopted approach, instead of treating the mixing coefficients of the Gaussian components as single parameters, it considers them as probability distributions. Under this framework, we need to estimate forms of probability distributions that best fit data properties instead of fitting an a priori known number of components to the captured data. Then, the Expectation-Maximization (EM) algorithm is adopted to estimate model parameters.

To compensate computational challenges arising from the nature of VI framework, we utilize conjugate priors and thus we derive analytical equations for model estimation. In this way, we avoid the need of any sampling method, which is computationally and memory inefficient.

Updating procedures are incorporated to allow dynamic model adaptation. Our updating method avoids the use of accumulated data from previous time instances, resulting in low memory requirements. Such a scheme assists the implementation of an in-camera module suitable for devices of low power and memory demands.

This paper is organized as follows: Section II introduces the VI framework for Gaussian mixture modeling of the background content, while Section III describes the algorithm for optimally estimating the model parameters. In Section IV, we present the EM optimization that best fits model parameters to the data statistical properties. A threshold independent on-line updating algorithm is introduced in Section V. Additionally, in this Section, a memory efficient implementation of the proposed VI-based background subtraction algorithm is presented allowing its use into reconfigurable in-camera hardware platforms of low-power and memory requirements. The in-camera reconfigurable architecture is discussed in Section VI, while experimental results are presented in Section VII using real-life thermal data streams. Finally, Section VIII draws the conclusions of the paper.

II. VARIATIONAL INFERENCE FOR GAUSSIAN MIXTURE MODELING

A. Gaussian Mixture Model Fundamentals

The Gaussian mixture distribution can be seen as a linear superposition of Gaussian functional components,

$$p(x|\boldsymbol{\varpi}, \boldsymbol{\mu}, \boldsymbol{\tau}) = \sum_{k=1}^K \varpi_k \mathcal{N}(x|\mu_k, \tau_k^{-1}), \quad (1)$$

where $\mathcal{N}(\cdot)$ represents the Gaussian distribution, K is the number of components, variables $\{\varpi_k\}_{k=1}^K$ refer to the mixing coefficients of each component satisfying $0 \leq \varpi_k \leq 1$ and $\sum_{k=1}^K \varpi_k = 1$. Variable x corresponds to the intensity of a pixel (i.e., the observed variable) and $\{\mu_k\}_{k=1}^K$, $\{\tau_k\}_{k=1}^K$ stand for the mean values and precisions of the Gaussian components respectively. By introducing a K -dimensional binary latent variable $\mathbf{z} = [z_1, \dots, z_K]$, in which a particular element is equal to one and all other elements are equal to zero, such as $\sum_{k=1}^K z_k = 1$ and $p(z_k = 1) = \varpi_k$, Eq. (1) can be written in terms of a marginal distribution $p(\mathbf{z})$ and a conditional distribution $p(x|\mathbf{z})$ as follows

$$p(x|\boldsymbol{\varpi}, \boldsymbol{\mu}, \boldsymbol{\tau}) = \sum_{\mathbf{z}} p(\mathbf{z}|\boldsymbol{\varpi}) p(x|\mathbf{z}, \boldsymbol{\mu}, \boldsymbol{\tau}), \quad (2)$$

where $p(\mathbf{z}|\boldsymbol{\varpi})$ and $p(x|\mathbf{z})$ are in the form of

$$p(\mathbf{z}|\boldsymbol{\varpi}) = \prod_{k=1}^K \varpi_k^{z_k}, \quad (3)$$

$$p(x|\mathbf{z}, \boldsymbol{\mu}, \boldsymbol{\tau}) = \prod_{k=1}^K \mathcal{N}(x|\mu_k, \tau_k^{-1})^{z_k}. \quad (4)$$

Eq. (2) models the effect of one sample. Given a set $\mathbf{X} = \{x_1, \dots, x_N\}$ of N pixel intensities (i.e., observed data), we conclude to a set of N latent variables, $\mathbf{Z} = \{z_1, \dots, z_N\}$. Each z_n is a K -dimensional binary vector with one element equals one and all the others equal zero, such as $\sum_{k=1}^K z_{nk} = 1$. Then, Eq. (3) and Eq. (4) are transformed to

$$p(\mathbf{Z}|\boldsymbol{\varpi}) = \prod_{n=1}^N \prod_{k=1}^K \varpi_k^{z_{nk}}, \quad (5)$$

$$p(\mathbf{X}|\mathbf{Z}, \boldsymbol{\mu}, \boldsymbol{\tau}) = \prod_{n=1}^N \prod_{k=1}^K \mathcal{N}(x_n|\mu_k, \tau_k^{-1})^{z_{nk}}. \quad (6)$$

The goal is to estimate a background model exploiting pixel intensities, that is, to calculate the values of $\boldsymbol{\varpi}$, $\boldsymbol{\mu}$ and $\boldsymbol{\tau}$, involved in the probability $p(x|\boldsymbol{\varpi}, \boldsymbol{\mu}, \boldsymbol{\tau})$.

B. Distribution Approximation through Variational Inference

In case that variable K of Gaussian components is a priori known, the values of $\boldsymbol{\varpi}$, $\boldsymbol{\mu}$ and $\boldsymbol{\tau}$ can be straightforward calculated using the methods of [21], [23]. For many real-life application scenarios, as the one this paper targets, it is better to let variable K fit the statistics of the data (i.e., let variable K be unknown). In such cases, one way to estimate K is to apply computationally expensive methods through sampling algorithms or to build several models of different number of components and then select the best one. An alternative computationally efficient approach, adopted in this paper, is to exploit the VI framework. More specifically, instead of treating the mixing coefficients $\boldsymbol{\varpi}$ as single parameters, which requires the knowledge of K , we treat them as probability distributions. This way, we are able to estimate the coefficients $\boldsymbol{\varpi}$ independently from K . Such an approach keeps computational complexity low since it avoids sampling methods or experimentation on different number of components.

Let us denote as $\mathbf{Y} = \{\mathbf{Z}, \boldsymbol{\varpi}, \boldsymbol{\mu}, \boldsymbol{\tau}\}$ a set which contains model parameters and the respective latent variables. Let us also denote as $q(\mathbf{Y})$ the variational distribution of \mathbf{Y} . Our objective is to estimate $q(\mathbf{Y})$ to be as close as possible to $p(\mathbf{Y}|\mathbf{X})$ for a given observation \mathbf{X} . Regarding similarity between two distributions, the Kullback-Leibler divergence,

$$KL(q||p) = \int q(\mathbf{Y}) \ln \frac{q(\mathbf{Y})}{p(\mathbf{Y}|\mathbf{X})} d\mathbf{Y}, \quad (7)$$

is adopted. $KL(q||p)$ is a non negative quantity, which equals zero only if $q(\mathbf{Y})$ is equal to $p(\mathbf{Y}|\mathbf{X})$. Thus, our goal is to minimize $KL(q||p)$.

In the context of the most common type of VI, known as *mean-field variational Bayes*, the variational distribution is assumed to be factorized over M disjoint sets such as $q(\mathbf{Y}) = \prod_{i=1}^M q_i(\mathbf{Y}_i)$. Then, as shown in [37], the optimal solution $q_j^*(\mathbf{Y}_j)$ that minimizes $KL(q||p)$ metric is given by

$$\ln q_j^*(\mathbf{Y}_j) = \mathbb{E}_{i \neq j} [\ln p(\mathbf{X}, \mathbf{Y})] + \mathcal{C}, \quad (8)$$

where $\mathbb{E}_{i \neq j} [\ln p(\mathbf{X}, \mathbf{Y})]$ is the expectation of the logarithm of the joint distribution over all variables that do not belong to the j^{th} partition and \mathcal{C} is a constant. Eq. (8) indicates the

presence of circular dependencies between the variables that belong to different partitions. Thus, estimating the optimal distribution over all variables suggests the exploitation of an iterative process such as the EM algorithm (see Section IV).

III. OPTIMAL DISTRIBUTIONS OVER MODEL PARAMETERS

In this section, we present the analytical form for the optimal distributions $q_j^*(Y_j)$, considering as the M disjoint sets the model coefficients and the latent variables; i.e., $q_Z^*(\mathbf{Z})$, $q_{\varpi}^*(\varpi)$, $q_{\tau}^*(\tau)$ and $q_{\mu}^*(\mu|\tau)$. For simplifying the notation, in the following the superscript of optimal distributions and the subscript for the j th partition are omitted.

A. Factorized Form of the Joint Distribution

To estimate $q(\mathbf{Y})$, we require to rewrite the right hand of Eq. (8), that is, the joint distribution $p(\mathbf{X}, \mathbf{Y})$, as a product

$$p(\mathbf{X}, \mathbf{Y}) = p(\mathbf{X}|\mathbf{Z}, \mu, \tau)p(\mathbf{Z}|\varpi)p(\varpi)p(\mu, \tau). \quad (9)$$

The distributions $p(\mathbf{X}|\mathbf{Z}, \mu, \tau)$ and $p(\mathbf{Z}|\varpi)$ are already known from Eq. (6) and Eq. (5). Thus, we need to define the prior distribution $p(\varpi)$ and the joint distribution $p(\mu, \tau)$. In this paper, conjugate priors [38] are adopted to estimate the distributions $p(\varpi)$ and $p(\mu, \tau)$. Such an approach is computational efficient since it avoids implementation of the expensive sampling methods yielding analytical solutions.

We start our analysis by the prior distribution $p(\varpi)$. In particular, since $p(\mathbf{Z}|\varpi)$ has the form of a multinomial distribution, [see Eq. (5)], its conjugate prior is given by

$$p(\varpi) = \frac{\Gamma(K\lambda_0)}{\Gamma(\lambda_0)^K} \prod_{k=1}^K \varpi_k^{\lambda_0-1}. \quad (10)$$

Eq. (10) is a Dirichlet distribution [39] with $\Gamma(\cdot)$ stands for the Gamma function and scalar λ_0 a control parameter. The smaller the value of λ_0 is, the larger the influence of the data rather than the prior on the posterior distribution $p(\mathbf{Z}|\varpi)$. The choice of setting the parameter λ_0 as a scalar instead of a vector of different values for each mixing coefficient is due to the fact that we adopt an uninformative prior framework, that is not preferring a specific component against the others.

Similarly, $p(\mu, \tau)$ is the prior of $p(\mathbf{X}|\mathbf{Z}, \mu, \tau)$ which is modeled through Eq. (6). The conjugate prior of (6) takes the form of a Gaussian-Gamma distribution [39], since both μ and τ are unknown. Subsequently, the joint distribution $p(\mu, \tau)$ can be modeled as

$$p(\mu, \tau) = p(\mu|\tau)p(\tau) \quad (11a)$$

$$= \prod_{k=1}^K \mathcal{N}(\mu_k|m_0, (\beta_0\tau_k)^{-1})\text{Gam}(\tau_k|a_0, b_0), \quad (11b)$$

where $\text{Gam}(\cdot)$ denotes the Gamma distribution. Again, an uninformative prior framework is adopted meaning that no specific preference about the form of the Gaussian components is given. The parameters m_0 , β_0 , a_0 and b_0 are discussed in Section IV-C.

In the following, the forms of optimal variational distributions are presented taken into consideration the results from Appendix A.

B. Optimal $q^*(\mathbf{Z})$ Distribution

Using Eq. (8) and the factorized form of Eq. (9), the distribution of the optimized factor $q^*(\mathbf{Z})$ is given by a Multinomial distribution of the form

$$q^*(\mathbf{Z}) = \prod_{n=1}^N \prod_{k=1}^K \left(\frac{\rho_{nk}}{\sum_{j=1}^K \rho_{nj}} \right)^{z_{nk}} = \quad (12a)$$

$$= \prod_{n=1}^N \prod_{k=1}^K r_{nk}^{z_{nk}}, \quad (12b)$$

where quantity ρ_{nk} is given as

$$\rho_{nk} = \exp \left(\mathbb{E}[\ln \varpi_k] + \frac{1}{2} \mathbb{E}[\ln \tau_k] - \frac{1}{2} \ln 2\pi - \frac{1}{2} \mathbb{E}_{\mu, \tau} [(x_n - \mu_k)^2 \tau_k] \right). \quad (13)$$

Due to the fact that $q^*(\mathbf{Z})$ is a Multinomial distribution we have that its expected value $\mathbb{E}[z_{nk}]$ will be equal to r_{nk}

C. Optimal $q^*(\varpi)$ Distribution

Using Eq. (9) and Eq. (8) the variational distribution of the optimized factor $q^*(\varpi)$ is given a Dirichlet distribution of the form

$$q^*(\varpi) = \frac{\Gamma(\sum_{i=1}^K \lambda_i)}{\prod_{j=1}^K \Gamma(\lambda_j)} \prod_{k=1}^K \varpi_k^{\lambda_k-1}. \quad (14)$$

Variable λ_k is equal to $N_k + \lambda_0$, while $N_k = \sum_{n=1}^N r_{nk}$ represents the proportion of data that belong to the k -th component.

D. Optimal $q^*(\mu_k|\tau_k)$ distribution

Similarly, the variational distribution of the optimized factor $q^*(\mu_k, \tau_k)$ is given by a Gaussian distribution of the form

$$q^*(\mu_k|\tau_k) = \mathcal{N}(\mu_k|m_k, (\beta_k\tau_k)^{-1}), \quad (15)$$

where the parameters m_k and β_k are given by

$$\beta_k = \beta_0 + N_k, \quad (16a)$$

$$m_k = \frac{1}{\beta_k} (\beta_0 m_0 + N_k \bar{x}_k). \quad (16b)$$

Variable \bar{x}_k is equal to $\frac{1}{N_k} \sum_{n=1}^N r_{nk} x_n$ and represents the centroid of the data that belong to the k -th component.

E. Optimal $q^*(\tau_k)$ distribution

After the estimation of $q^*(\mu_k|\tau_k)$, the variational distribution of the optimized factor $q^*(\tau_k)$ is given by a Gamma distribution of the following form

$$q^*(\tau_k) = \text{Gam}(\tau_k|a_k, b_k), \quad (17)$$

while the parameters a_k and b_k are given as

$$a_k = a_0 + \frac{N_k}{2}, \quad (18a)$$

$$b_k = b_0 + \frac{1}{2} \left(N_k \sigma_k + \frac{\beta_0 N_k}{\beta_0 + N_k} (\bar{x}_k - m_0)^2 \right), \quad (18b)$$

where $\sigma_k = \frac{1}{N_k} \sum_{n=1}^N (x_n - \bar{x}_k)^2$.

IV. DISTRIBUTION PARAMETERS OPTIMIZATION

In Section III, we derive approximations of the random variable distributions. Then, the EM algorithm is employed to optimally estimate the coefficient distributions that best fit the observations. Since the statistics of the observed data are not a priori known, both prior and model parameters are dynamically estimated from the observed data.

A. The EM Optimization Framework

E-Step: Let us assume the t -th iteration of the EM optimization algorithm. Then, during the E-step, only the value of r_{nk} is readjusted according to the statistics of the currently available observed data. Variable r_{nk} actually expresses the degree of fitness of the n -th datum to the k -th cluster, as derived from Eq. (12). Due to the fact that $q^*(\varpi)$ is a Dirichlet distribution and $q^*(\tau_k)$ is a Gamma distribution, the following holds

$$\ln \tilde{\tau}_k(t) \equiv \mathbb{E}[\ln \tau_k(t)] = \Psi(a_k(t)) - \ln b_k(t), \quad (19a)$$

$$\ln \tilde{\varpi}_k(t) \equiv \mathbb{E}[\ln \varpi_k(t)] = \Psi(\lambda_k(t)) - \Psi\left(\sum_{k=1}^K \lambda_k(t)\right), \quad (19b)$$

$$\mathbb{E}[\tau_k(t)] = \frac{a_k(t)}{b_k(t)}, \quad (19c)$$

where $\Psi(\cdot)$ is the digamma function. In Eq. (19), we set $\ln \tilde{\tau}_k(t) \equiv \mathbb{E}[\ln \tau_k(t)]$ and $\ln \tilde{\varpi}_k(t) \equiv \mathbb{E}[\ln \varpi_k(t)]$ to simplify the notation of the following equations. Then,

$$r_{nk}(t+1) \propto \tilde{\varpi}_k(t) \tilde{\tau}_k(t)^{1/2} \exp\left(-\frac{a_k(t)}{2b_k(t)}(x_n - m_k(t))^2 - \frac{1}{2\beta_k(t)}\right) \quad (20)$$

by substituting Eq. (19) into Eq. (13) and using Eq. (12). In Eq. (20), $r_{nk}(t+1)$ expresses the degree of fitness of the n -th datum to the k -th cluster at the next $t+1$ iteration of the algorithm.

M-Step: During the M-step, we keep fixed the value of $r_{nk}(t)$, as it has been calculated through the E-Step. Then, we update the values of the background model coefficients, which we will allow us to re-estimate the degree of fitness r_{nk} at the next iteration stage, exploiting Eq. (20).

Particularly, initially, the parameters $N_k(t+1)$ and $\lambda_k(t+1)$ are estimated, based on the statements of Section III-C and the $r_{nk}(t+1)$ of (20),

$$N_k(t+1) = \sum_{n=1}^N r_{nk}(t+1), \quad (21a)$$

$$\lambda_k(t+1) = N_k(t+1) + \lambda_0. \quad (21b)$$

It has to be mentioned that these are the only variables that are needed for updating model parameters, i.e. ϖ , μ and τ , using Eq. (14), Eq. (15) and Eq. (17).

The distribution $q^*(\varpi(t+1))$ of the background model coefficients is computed based on Eq. (14). The value λ_0 is given in Section IV-C. We recall that in our approach, the number of Gaussian components that the background content

is composed of is not a priori known. For this reason, we have treated the mixing coefficients of the background model as probability distributions and not as single parameters. Such an approach provides us the ability of initializing the EM algorithm by setting the number of clusters to be smaller or equal to a maximum available value, coinciding with the number of observed data, that is, $K_{max} \leq N$. Then, the probability coefficients distributions re-arrange the number of clusters in order to best fit the statistics of the observations. This is achieved through EM optimization.

In the following, the parameters $a_k(t+1)$ and $b_k(t+1)$ are updated to define the Gamma distribution of $q^*(\tau_k(t+1))$ that best fit the observations through Eq. (18). Again, the priors a_0 , b_0 and β_0 are given in Section IV-C. The distribution of $\tau_k(t+1)$ is a parameter of the Gaussian components of the background model affecting the variance of k -th cluster.

Next, the distribution $q^*(\mu_k(t+1)|\tau_k(t+1))$ is updated exploiting $\tau_k(t+1)$. In order to do this, we need to update $\beta_k(t+1)$ and $m_k(t+1)$ based on Eq. (16). This way, we can update model parameters of the Gaussian components that mixes the background triggering next iteration stages of the EM as in Eq. (20). The E and M steps are repeated sequentially until the values for model parameters are not significantly changing. As shown in [40] convergence of EM algorithm is guaranteed because bound is convex with respect to each of the factors $q(\mathbf{Z})$, $q(\varpi)$, $q(\mu|\tau)$ and $q(\tau)$.

During model training the mixing coefficient for some of the components takes value very close to zero. Components with mixing coefficient less than $1/N$ are removed (we require each component to model at least one observed sample) and thus after training, the model has automatically determined the right number of Gaussian components.

B. Initialization Aspects

The k-means++ algorithm [41] is exploited to initialize the EM algorithm at $t = 0$. The k-means++ presents advantages compared to the conventional k-means since it is less depended on initialization. The k-means++ creates an initial partition of the data, which is used to initialize EM algorithm. Then, at the updating stages of the algorithm (see Section IV-A), the probabilities of each observed datum (image pixel intensity) to belong to one of the K_{max} available clusters, expressed through r_{nk} , are updated. This way, the final number of clusters are dynamically refined according to the statistical distributions of the image pixel intensities.

Let us denote as $\hat{N}_k = N_k(t = 0)$ the number of observations that belong to k -th cluster at the $t = 0$ iteration. Then, an initial estimate of the model coefficients is $\varpi_k(t = 0) = \hat{N}_k/N$, meaning that the significance of each Gaussian component is proportional to the number of data that belong to the k -th cluster. Thus, the initialization of $\lambda_k(t = 0) = N\varpi_k(t = 0) + \lambda_0$, [see Eq. (14)] expresses the number of observations associated with each component.

The parameters $a_k(t = 0)$, $b_k(t = 0)$, $\beta_k(t = 0)$ and $m_k(t = 0)$ are initially estimated from Eq. (18) and Eq. (16), considering the knowledge of the priors parameters as discussed in Section IV-C. Finally, the model parameter $\tau_k(t = 0)$ is

given as inverse proportional of the variance of the data of the k -th initial cluster, that is, $\tau_k(t=0) = \hat{v}_k^{-1}(t=0)$.

C. Priors Parameters

The parameter λ_0 in Eq. (10) can be interpreted as the effective prior number of observations associated with each component. However, we do not have any prior information regarding this number. In order to use an uninformative prior and maximize the influence of the data over the posterior distribution we set $\lambda_0 = 1$, see [42].

Equations Eq. (18a) and Eq. (18b) suggest that the values of parameters a_k and b_k are primarily affected by the data and not by the prior, when the values of the parameters a_0 and b_0 are close to zero. For this reason we set a_0 and b_0 to a very small value (10^{-3} in our implementation).

Similarly, we initialize m_0 as the mean value of the observed data and precision $\beta_0 = \frac{b_0}{a_0 v_0}$, where v_0 is the variance of the observed data. We use uninformative priors, since we do not have any information regarding neither the number of components nor their true mean and variance values.

V. ONLINE UPDATING MECHANISM AND BACKGROUND SUBTRACTION

Using the aforementioned approach, we fit a model to the background considering a pool of N observed data. In this section, an adaptive strategy that is threshold-independent and memory efficient is presented. Such an approach permits implementation of the proposed algorithm to an in-camera hardware embedded architecture of low power and memory requirements. This way we deliver thermal sensors embedding with the capability of detecting moving objects in real-time.

Let us denote as x_{new} a new observed sample. Then, a decision is made whether x_{new} can be approximated by our best fitted model or not. For this reason, the best matched Gaussian component c to x_{new} is estimated by minimizing the Mahalanobis distance D_k ,

$$c = \arg \min_k D_k = \arg \min_k \sqrt{(x_{new} - \mu_k)^2 \tau_k}, \quad (22)$$

where μ_k and τ_k stand for the mean and precision of the k -th component. We use Mahalanobis distance, since this is a reliable distance measure between a point and a distribution. Then, x_{new} belongs to c with probability

$$p(x_{new} | \mu_c, \tau_c) = \mathcal{N}(x_{new} | \mu_c, \tau_c^{-1}). \quad (23)$$

A. Threshold Independent

Conventionally, Eq. (23) implies a threshold to determine the probability limit over which the new sample x_{new} belongs to c . To overcome threshold limitations, the following adaptive approach is adopted in this paper.

Let us denote as Ω the image pixel responses over a fixed time span. Then, we model the probability to observe the new sample x_{new} in a region of range 2ϵ centered at x_{new} as

$$p(x_{new}; \epsilon) = \frac{N_\epsilon}{N} \mathcal{U}(x_{new}; x_{new} - \epsilon, x_{new} + \epsilon), \quad (24)$$

where $N_\epsilon = |\{x_i \in \Omega : x_{new} - \epsilon \leq x_i \leq x_{new} + \epsilon\}|$ is the cardinality of the set that contains samples ϵ -close to x_{new} and $\mathcal{U}(x_{new}; x_{new} - \epsilon, x_{new} + \epsilon)$ is a Uniform distribution with lower and upper bounds that equal to $x_{new} - \epsilon$ and $x_{new} + \epsilon$ respectively.

Eq. (24) suggests that the probability to observe the x_{new} is related to the portion of data that have been already observed around x_{new} . By increasing the neighborhood around x_{new} , i.e., increasing the value of ϵ , the quantity $\mathcal{U}(x_{new}; x_{new} - \epsilon, x_{new} + \epsilon)$ is decreasing, while the value of N_ϵ is increasing. Therefore, we can estimate the optimal range ϵ^* around x_{new} that maximizes Eq. (24)

$$\epsilon^* = \arg \max_\epsilon p(x_{new}; \epsilon). \quad (25)$$

Based on the probabilities $p(x_{new} | \mu_c, \tau_c)$ and $p(x_{new}; \epsilon^*)$, which are exclusively derived by the observations, we can define our decision making mechanism. Concretely, if

$$p(x_{new} | \mu_c, \tau_c) \geq p(x_{new}; \epsilon^*) \quad (26)$$

the new observed sample x_{new} can sufficiently represented by our model, i.e., the value of the new observed sample is sufficiently close to an existing Gaussian component. Otherwise, a new Gaussian component should be created, since the value of x_{new} will not be close to what the model has already learnt.

B. Model Updating

When the value of the new observed sample is sufficiently close to an existing Gaussian component, the parameters of the mixture are being updated using the *following the leader* [43] approach described as

$$\varpi_k \leftarrow \varpi_k + \frac{1}{N} (o_k - \varpi_k), \quad (27a)$$

$$\mu_k \leftarrow \mu_k + o_k \left(\frac{x_{new} - \mu_k}{\varpi_k N + 1} \right), \quad (27b)$$

$$\sigma_k^2 \leftarrow \sigma_k^2 + o_k \left(\frac{\varpi_k N (x_{new} - \mu_k)^2}{(\varpi_k N + 1)^2} - \frac{\sigma_k^2}{\varpi_k N + 1} \right), \quad (27c)$$

where $\sigma_k^2 = \tau_k^{-1}$ is the variance of the k -th component. The binary variable o_k takes value one when $k = c$ and zero otherwise.

When the new observed sample cannot be modeled by any existing component, i.e. the value of the new sample will not be close to what the model has already learnt [see Eq. (26)], a new component is created with mixing coefficient ϖ_{new} , mean value μ_{new} and standard deviation σ_{new} , defined as

$$\varpi_{new} = \frac{1}{N}, \quad (28a)$$

$$\mu_{new} = x_{new}, \quad (28b)$$

$$\sigma_{new}^2 = \frac{(2\epsilon)^2 - 1}{12}. \quad (28c)$$

Variable σ_{new}^2 is estimated using the variance of the Uniform distribution. From Eq. (28), we derive that $\varpi_{new} = 1/N$ since it models only one sample (the new observed one), its mean value equals the value of the new sample and its variance

the variance of the Uniform distribution, whose the lower and upper bounds are $x_{new} - \epsilon$ and $x_{new} + \epsilon$ respectively. When a new component is created the values for the parameters for all the other components remain unchanged except from the mixing coefficients $\{\varpi_k\}_{k=1}^K$ which are normalized to sum $\frac{N-1}{N}$. Then, the components whose mixing coefficients are less than $\frac{1}{N}$ are removed, since they model less than one sample, and the mixing coefficients of the remaining components are re-normalized.

C. Memory Efficient Implementation

The main limitation of the aforementioned threshold independent approach is that it requires the storage of several observations in order to reliably estimate the probability $p(x_{new}; \epsilon^*)$. In this section, we introduce a framework of updating the model parameters of the background content without the need of storing observations. This reduces memory requirements and thus it is a crucial step towards implementing our proposed system on devices of low power and memory requirements.

We recall that we have denoted as c the closest component, in terms of a Mahalaobis distance, to the new observed datum x_{new} . This component is a Gaussian distribution with mean value μ_c , precision τ_c and mixing coefficient ϖ_c . Therefore, the quantity N_ϵ can be approximated as

$$N_\epsilon \approx \tilde{N}_\epsilon = N\varpi_c \int_{x_{new}-\epsilon}^{x_{new}+\epsilon} \mathcal{N}(t|\mu_c, \tau_c^{-1}) dt. \quad (29)$$

Denoting as

$$G_c(x) = \int_{-\infty}^x \mathcal{N}(t|\mu_c, \tau_c^{-1}) dt \quad (30)$$

the cumulative Gaussian distribution of the closest Gaussian component and using Eq. (29), \tilde{N}_ϵ is equal to

$$\tilde{N}_\epsilon = N\varpi_c (G_c(x_{new} + \epsilon) - G_c(x_{new} - \epsilon)) \quad (31)$$

Then, the probability $p(x_{new}; \epsilon)$ is approximated as

$$\begin{aligned} p(x_{new}; \epsilon) &\approx \tilde{p}(x_{new}; \epsilon) = \\ &= \frac{\tilde{N}_\epsilon}{N} \mathcal{U}(x_{new}; x_{new} - \epsilon, x_{new} + \epsilon). \end{aligned} \quad (32)$$

Probability $\tilde{p}(x_{new}; \epsilon)$ is a continuous and unimodal function with a global maximum. Therefore, ϵ^* can be found by setting the first derivative of Eq. (32) equal to zero. After the estimation of ϵ^* , we can compute $\tilde{p}(x_{new}; \epsilon^*)$. Thus, we are able to update the mixture model by comparing $\tilde{p}(x_{new}; \epsilon^*)$ to $p(x_{new}|\mu_c, \tau_c)$ [see Eq. (26)].

D. Background Subtraction

Let us denote as bg and fg the classes of background and foreground pixels respectively. The aforementioned modeling process actually approximates the probability $p(x|bg)$. However, our goal is to calculate the probability $p(bg|x)$ in order to model the background content based on a set of observations. Then, the foreground object is derived through a subtraction process. Hence the Bayes rule is applied;

$$p(bg|x) = \frac{p(x|bg)p(bg)}{p(x|bg) + p(x|fg)}. \quad (33)$$

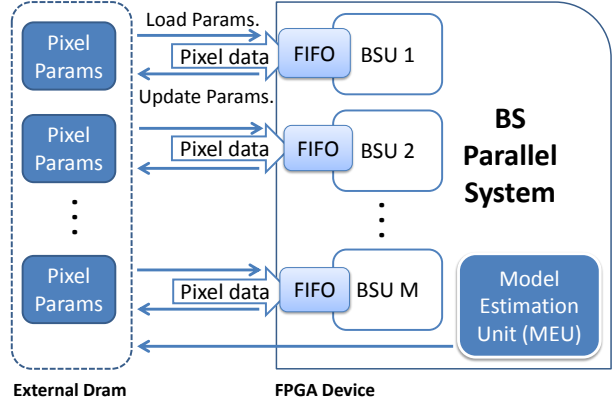


Fig. 1. The data loading process of the Background Subtraction Parallel System (BSPS).

The unknown factors of Eq. (33) are $p(bg)$ and $p(x|fg)$. The probability $p(bg)$ corresponds to the prior probability of background class. In our case, we have set it to be 1/2 due to the uninformative assumption framework. The probability $p(x|fg)$ is modelled as uniform distribution as in [25]. The overview of the proposed scheme is shown in Algorithm 1.

Algorithm 1: Overview of Background Subtraction

- 1: capture N frames
- 2: create N -length history for each pixel
- 3: initialize parameters (see Section IV)
- 4: **until** convergence (training phase: Section IV)
- 5: compute r_{nk} using (20)
- 6: recompute parameters using (14), (16) and (18)
- 7: **for each** new captured frame
- 8: classify each pixel as foreground or background (see subsection V-D)
- 9: update background model (see subsection V-C)

VI. IN-CAMERA ACCELERATION ARCHITECTURE

In this section, we describe in detail the hardware architecture for the proposed background subtraction algorithm. We call the proposed parallel implementation as Background Subtraction Parallel System (BSPS). BSPS exploits the reconfigurable resources of today's FPGA devices.

A. High Level Architecture

Since the proposed approach makes no assumption for pixel relationships, the background model for all pixels can be computed independently. Thus, our hardware architecture consists of many parallel cores in a scalable configuration, each processing a single pixel. In Section VII we demonstrate two configurations; one low cost, featuring a 4-core BSPE Engine and a second one featuring a 16-core BSPE Engine.

Each of the cores is connected to a shared bus in order to get the processing data from the external DRAM (or memory mapped camera module) of a host system. The data loading is performed in batches of up to 16 pixels as shown in Fig.1.

All operations are per pixel with no dependencies between them. Thus using a buffering scheme and utilizing simple FIFOs, we can hide the latency of the external DRAM

and make our scheme working seamlessly as a streaming accelerator. The operations regarding data loading and write-back are fully pipelined. More details regarding the bandwidth demands are given in Section VII. The output of each core is a probabilistic classification for the corresponding pixel (background or foreground) and the updated parameters of the background model.

B. System Organization

The BSPS comprises of two basic sub-modules: the *Model Estimation Unit* (MEU), which is depicted in Fig.2 and the *Background Subtraction Unit* (BSU) depicted in Fig.3. The MEU is activated just once at the initialization process of the system. It is responsible for building the proposed background model at all pixel locations. It uses a small history of pixel values (~ 100 initial captured frames) and automatically estimates the appropriate number of Gaussian components along with their mixing coefficients. After the model is built the MEU stores the model parameters to the external DRAM for each one of the image pixels.

Then and during the normal operation of the system, only the BSU is activated. The BSU takes as input the pixel data stream along with the model parameters and gives as output the probabilistic segmentation of each pixel (see subsection V-D), while it also updates model parameters (see subsection V-C). This way for each pixel location (x, y) , a background model is maintained and updated, which is utilized for the classification of all the new incoming pixels from the data stream.

C. The Model Estimation Unit

One of the key advantages of the proposed scheme is that it does not require any prior knowledge about the structure of the background model in order to achieve an optimal operation. The MEU, depicted in Fig.2, is responsible for this task, which builds an accurate model for the specific background and its inherent temporal characteristics. It takes as input a small history of pixel responses (~ 100) at a specific pixel location and outputs an accurate background model for this pixel. As mentioned in Section IV two basic algorithms are utilized in this module: the k-means++ and the EM algorithm.

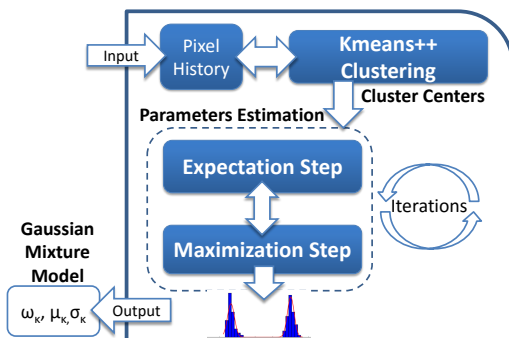


Fig. 2. The Model Estimation Unit (MEU) organization.

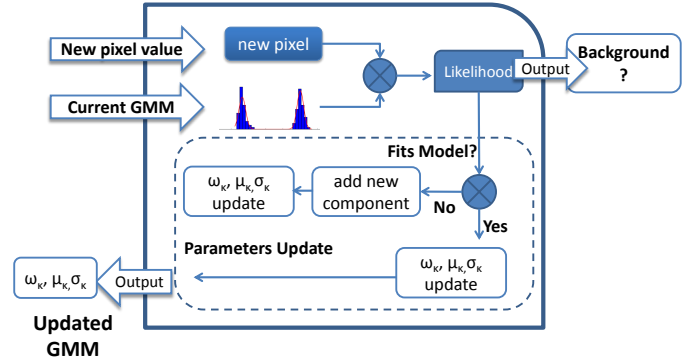


Fig. 3. The Background Subtraction Unit (BSU) organization.

D. The Background Subtraction Unit

The BSU, described in Fig.3, is responsible for classifying the incoming pixels into the two available classes (background and foreground) and also updating the background model according to the new pixel response. For this reason, BSU takes as input a new pixel value (x_{new}) and the current Gaussian mixture for this pixel, which is stored outside the chip, and gives as output the updated Gaussian mixture, as well as, the probabilistic classification of the incoming pixel.

VII. EXPERIMENTAL VALIDATION

A. VI Mixture Model Fitting Capabilities

During experimental validation, we evaluate the Variational Inference Mixture Model (VIMM) in terms of fitting accuracy and computational cost. We compare VIMM with the conventional Gaussian Mixture Model (GMM) and Dirichlet Process Mixture Model (DPMM). The GMM are employed under three different settings; (i) the right number of components, (ii) with more and (iii) less components than the underlying distribution.

Initially and for experimentation purposes only, we create two synthetic datasets each of 200 samples. The first set is generated from two different Gaussian distributions, with mean values 15 and 35, variance 1.5 and 2.0 and proportions 8/15 and 7/15 of data respectively. The second set contains samples from three different Gaussian distributions, with mean values 15, 35 and 55, variance 1.5, 2.0 and 2.5 and proportions 4/15, 4/15 and 7/15 of data respectively.

In all cases the initial value for the number of components for VIMM is set to 10, and then we let the proposed fitting procedure to estimate the appropriate number of components that characterize the underlying distribution. In order to compare our method with the conventional GMMs of fixed number of components, we create two Gaussian models of 10 and 2 components respectively. These numbers are arbitrarily chosen, since the correct number of components is not a priori known.

Figure 4 and 5 presents the fitting performance on the first and second dataset respectively. As is observed, our method correctly estimates the number of components for both datasets. The GMM with 10 components fits well the data that come from the first dataset, but it under-fits the data coming

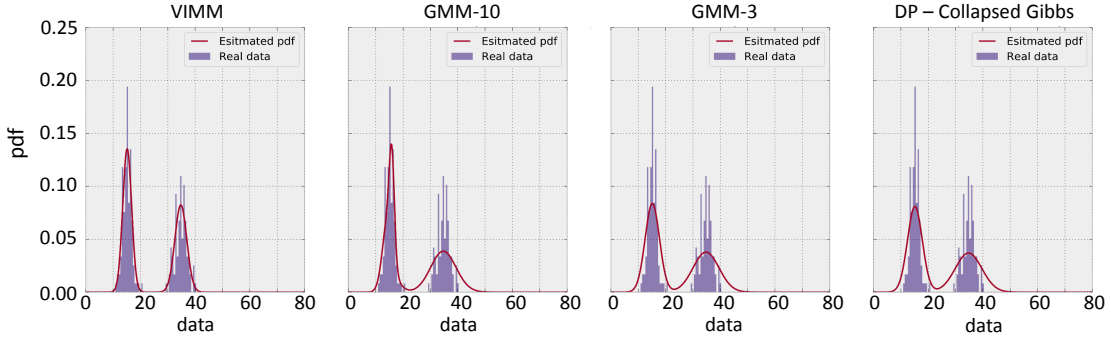


Fig. 4. Fitting performance – two Gaussian distributions.

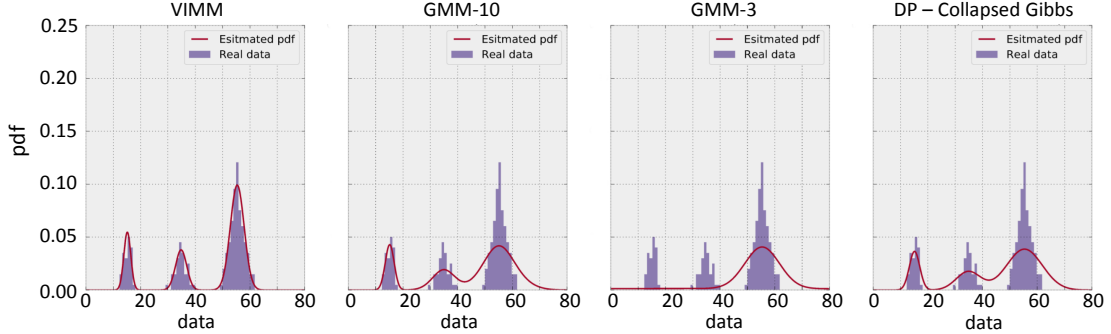


Fig. 5. Fitting performance – three Gaussian distributions.

TABLE I
TIME PERFORMANCE OF THE DIFFERENT MODELS IN SECONDS.

	VIMM	GMM-10	GMM-2	DPMM
First dataset	0.156	0.034	0.011	21.35
Second dataset	0.124	0.067	0.031	30.19

from the second set. This means that it fails to be adapted to the statistical variations of the data. The DPMM approach yields better results, since it is able to be adapted to the current data statistics, but it still under-fits the data.

Finally, Table I presents time performance of the different models. It has to be mentioned that all presented times were computed in Python and not in hardware implementation. The time requirements regarding the hardware implementation are presented in subsection VII-D. The conventional GMMs present the best time performance due to their simplicity. Our method is 2 to 5 times slower than conventional GMMs. However, it is much faster than the DPMM, which is more than 135 times slower than our model.

B. Updating Mechanism Performance

In this section we evaluate the quality of the proposed updating mechanism, with and without keeping in memory the observed data, by comparing it against the updating mechanism presented in [23]. The rationale behind the decision to explore both cases lies in the fact that we target special purpose hardware (i.e in-camera hardware accelerator) with very limited on-chip memory. In this respect we have

to validate that even without keeping the observed data in memory the algorithm performance is not affected at all.

Fig. 6 presents the adaptation of our model to new observations (Fig. 6(a) and Fig. 6(b)) and the model presented in [23] (Fig. 6(c)). To evaluate the quality of the adaptation of the models, we use a toy dataset with 100 observations. Observed data were generated from two Gaussian distributions with mean values 16 and 50 and standard deviations 1.5 and 2.0 respectively. The initially trained models are presented in the left column. Then, we generated 25 new samples from a third Gaussian distribution with mean value 21 and standard deviation 1.0. The middle column indicates the adaptation performance after 25 new observations, while the right column after 50. Our model, either it uses the history of observed data or not, creates a new component and successfully fits the data. On the contrary, the model of [23] is not able to capture the statistical relations of the new observations and fails to separate the data generated from distributions with mean values 16 and 21 (see the middle and right column). The quality of the presented updating mechanism becomes more clear in the right column, which presents the adaptation of the models after 50 new observations.

C. Background Subtraction Algorithm Evaluation

For evaluating our algorithm, we use the Ohio State University (OSU) thermal datasets and a dataset captured at Athens International Airport (AIA) during eVacuate¹ European Union funded project. Specifically, we used two OSU datasets, referred as OSU1 and OSU2, which contain frames that have

¹<http://www.evacuate.eu>

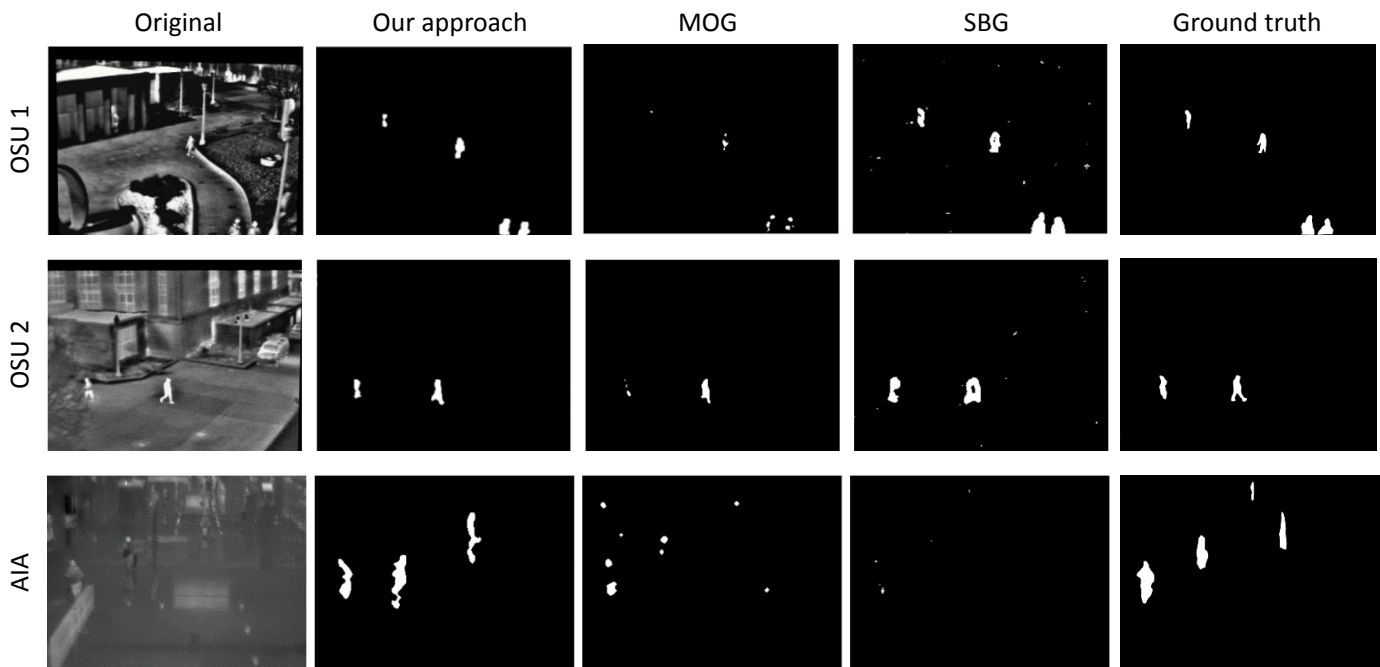


Fig. 7. Visual results for all datasets.

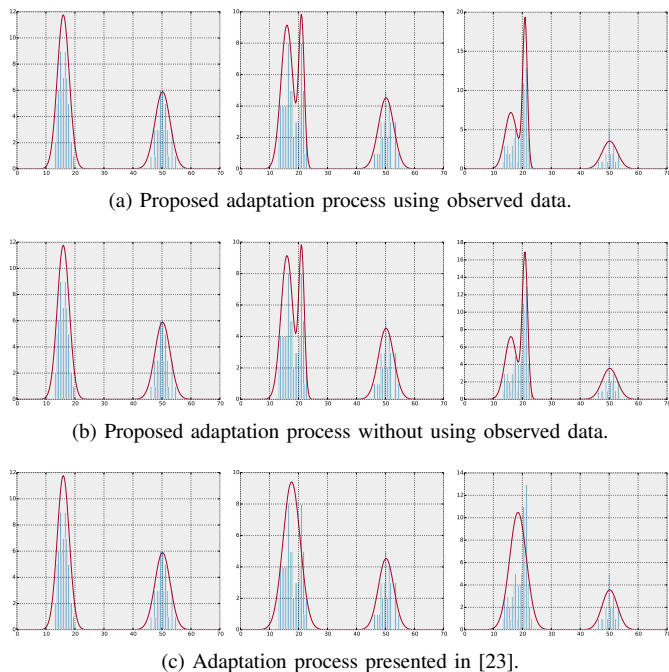


Fig. 6. Performance evaluation of model updating mechanisms.

been captured using a thermal camera and have been converted to grayscale images. On the contrary, the AIA dataset contains raw thermal frames whose pixel values correspond to the real temperature of objects.

OSU datasets [26], [3], [27] are widely used for benchmarking algorithms for pedestrian detection and tracking in thermal imagery. Videos were captured under different illumination and weather conditions. AIA dataset was captured using a Flir A315 camera at different Airside Corridors and the Departure Level. Ten video sequences were captured, with frame size

320×240 pixels of total duration 32051 frames, at 7.5fps, that is, about 1h and 12mins. The experimentation was conducted throughout the third pilot scenario of eVacuate project.

We compared our method against the method presented by Zivkovic in [23] (MOG), which is one of the most robust and widely used background subtraction techniques. MOG algorithm uses a pre-defined number of Gaussian components for building the background model. In order to perform a fair comparison we fine-tune the parameters of MOG algorithm for each of the two datasets to optimize its performance. Furthermore, we compare our method against the method of [3], [27] (SBG) used for background subtraction in thermal data. This method uses a single Gaussian distribution for modeling the background and, thus, it often under-fits the background. Comparison against this technique can highlight problems that arise when the number of components of a GMM is underestimated. It has to be mentioned that we do not compare our method against a DPMM-based background subtraction technique, like the one presented in [25], since its computational cost is high and we target low power and memory devices.

Fig. 7 visually present the performance of the three methods. As is observed, our method outperforms both MOG and SBG on all datasets. While MOG and SBG perform satisfactory on grayscale frames of OSU datasets, their performance collapses when they applied on AIA dataset, which contains actual thermal responses, due to their strong assumptions regarding the distribution of the responses of pixels and the peculiarities of thermal imagery i.e. high signal-to-noise ratio, lack of color and texture and non-homogeneous thermal responses of objects (see Section I). Then, an objective evaluation takes place. For this reason, we utilize the objective metrics of *recall*, *precision* and *F1 score*. Regarding OSU datasets, MOG

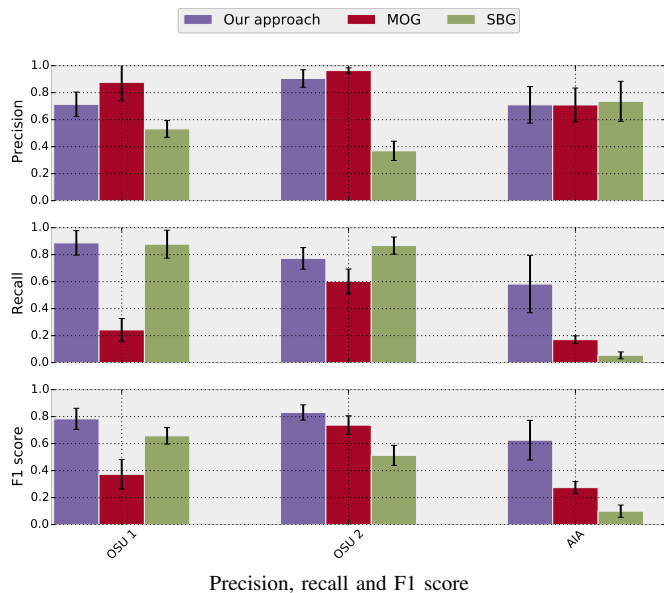


Fig. 8. Algorithms performance per dataset.

algorithm presents high precision, however, it yields very low recall values, i.e. the pixels that have been classified as foreground are indeed belong to the foreground class, but a lot of pixels that in fact belong to background have been misclassified. SBG algorithm seems to suffer by the opposite problem. Regarding AIA dataset, our method significantly outperforms both approaches. In particular, while MOG and SBG algorithms present relative high precision, their recall values are under 20%. Figure 8 presents average precision, recall and F1 score per dataset and per algorithm to give an objective evaluation.

Regarding computational cost, the main load of our algorithm is in the implementation of EM optimization. In all experiments conducted, the EM optimization converges within 10 iterations. Practically, the time required to apply our method is similar to the time requirements of Zivkovic’s method making it suitable for real-time applications.

D. Hardware Cost

The BSPS presented in this work is completely scalable in terms of parallel pixel cores so as to accommodate the exact cost and performance needs of the target application.

The main argument of this work is that a novel highly accurate and demanding algorithm that needs to run in a 24/7 basis could be handled very efficiently by a reconfigurable device running as an in-camera accelerator. Thus we primarily demonstrate our system in a low cost Xilinx Atrix7 FPGA device (xc7a200tfbg484-3). In addition we deploy our system in a more powerful Virtex7 device (xc7vx550tffg1158-3) to show that it seamlessly scales to support more parallel cores.

For the code synthesis and bitstream generation we used Xilinx Vivado and Vivado HLS. For validation and proof only purposes our system was implemented in a low end Zedboard evaluation platform² powered by a small Xilinx Zynq device.

²“Zedboard Evaluation Board”– <http://zedboard.org/>.

TABLE II
TYPICAL HARDWARE COST ON LOW COST, LOW POWER XILINX ARTIX7 DEVICE (XC7A200TFBG484-3). 4-BSU CORES/1-MEU CORE.

Logic Utilization	Used	Available	Utilization
Number of Flip Flops	143089	269200	53%
Number of Slice LUTs	119964	129000	92%
Number of DSP48E	506	740	68%
Number of Block RAM_18K	20	730	2%

TABLE III
TYPICAL HARDWARE COST ON XILINX VIRTEX 7 DEVICE (XC7VX550TFFG1158-3). 16-BSU CORES/1-MEU CORE.

Logic Utilization	Used	Available	Utilization
Number of Flip Flops	241604	692800	35%
Number of Slice LUTs	269004	346400	78%
Number of DSP48E	1184	2880	41%
Number of Block RAM_18K	14.50	1180	1.2%

Table II shows the hardware utilization for the Artix7 device when implementing 4 BSU cores and 1 MEU core of the proposed system. The reason behind implementing only 1MEU is that this unit operates only for the initialization and parameter estimation of the system and thus its performance is not crucial.

From the same table it is shown that the critical resource is the LUTs and DSPs. This is explained as the operations involved in the algorithm are mostly multiplications and divisions and thus apart from the DSPs, additional logic and signals are necessary to route the intermediate results and handle all algorithm states. DRAM utilization is almost zero as all operations are per pixel and no further caching in data is necessary, due to the fact that there is no requirement for keeping the observed data in memory (Section VII-B). At this point it should be mentioned that keeping the observed data in memory would prohibit the implementation of this algorithm in low memory devices.

Table III shows the hardware utilization of the Virtex 7 device when implementing 16 BSU cores and 1-MEU core of our scheme. The resource utilization in this case follows the same reasoning as before.

The above two hardware configurations are compared with a quad-core ARM Cortex A9 CPU (Exynos4412 SoC) clocked at 1.7 GHz with 2GB RAM and a low power mobile Intel i5 (2450M) Processor clocked at 2.5Ghz with 8GB RAM. Intel processor features two physical cores with hyper threading capability (4 threads in total). It is selected for the evaluation as it offers a competitive computation power per watt.

For the Intel i5 the software compiler platform used was Microsoft Visual Studio 2012 and our code was optimized for maximum speed (-O2 optimization level). For the ARM A9 platform was used a lightweight XUbuntu 13.10 operating system with a g++ compiler using -O2 and-O3 optimization level (O3 wasnt improving performance at all). In all software reference implementations OpenMP was also used to utilize all the available cores/threads of the platform.

TABLE IV
COMPARISON TABLE BETWEEN A XILINX ATRIX7 DEVICE @210MHZ, A XILINX VIRTEX7 DEVICE @ 222 MHZ, AN INTEL I5 @2.5GHZ AN ARM CORTEX A9 @1.7GHZ AND A DSP @ 600MHZ.

Image frame	320 × 240	640 × 480	μJ/pixel
Artix 7 4-cores	17.36 fps	4.34 fps	3.45
Vertex 7 16-cores	69.88 fps	17.47 fps	3.49
ARM A9 4-cores	8.27 fps	2.07 fps	4.7-6.2
Intel i5 2-cores/ 4-threads	58.59 fps	14.56 fps	5.82
MOG [23] Blackfin BF-537 DSP	3.57 fps	-	-

For the FPGA we measure the exact clock cycles needed for segmenting a single pixel by a single core including loading and write back cycles. For this purpose we use the Zedboard evaluation board. The exact clock cycles measured between 700-830 when real datasets are evaluated. These measurements are also verified for the proposed Atrix7 and Virtex7 devices using post-place and route timing simulation.

Considering the I/O latency between the DRAM and the FPGA, it is completely hidden as the operations for each core are depending only on a single pixel and its corresponding background model. All this information it is encoded in about 256 bits in average, thus a buffering scheme using simple FIFOs it is easily implemented. The bandwidth demands between the device and the DRAM is no more than 250 MB/sec for 25FPS at 640x480 resolution which is easily achievable even from low-end FPGA devices.

In all the experiments for the Intel i5 and ARM A9 we start measuring latency times after the data are loaded in the DRAM of the CPU. This probably is in benefit of the CPUs as the cache is hot in most of the measured cases. Several experiments are conducted and average values are calculated.

Table IV shows that implementing just 4-cores in the Atrix7 device we get 17.3 FPS at 320x240 exceeding by far the capabilities of the FLIR A-315 thermal camera. The 4-core FPGA design outperforms the ARM A9 quad core CPU giving twice the FPS. In terms of power Atrix7 consumes 4.6 watts based on Vivado’s Power analysis tool while quad core ARM A9 consumes about 3.5-4 watts³. As expected the Intel i5 utilizing 4-threads outperforms the two previous platforms offering also the best performance per core. Its consumption is measured at 26.2watts⁴ and refers only to the CPU consumption. Moving to the Virtex 7 device, we see that it offers better performance than the Intel i5, as it is capable of fitting 16-BSU cores. In terms of power the Virtex7 consumes 18.6 Watts measured using Vivado’s Power analysis tool.

Looking at the energy metric J/pixel in Table IV, both FPGA devices give similar J/pixel and also better than the Intel i5. For the ARM A9 this metric is expressed as a range as it is based mostly on specs. In our evaluation experiments we could measure the total dynamic power of the board using the

³No accurate measurement separately for the CPU cores is possible as Odroid U3 evaluation board doesn’t offer on-chip power meters.

⁴Measurements are performed using Intel’s Power Gadget 3.0 Tool utilizing Intel’s on-chip power meters.

ODROID smart Power5 but it is not possible to safely measure only the CPU core modules.

The last column in Table 3 refers to the work of [44] which implements the original MOG algorithm in an in-camera DSP processor (Blackfin BF-537) as a reference design for his proposed scheme. Even though it is hard to make a direct comparison, we see how challenging for embedded processors is it to keep up with the demanding task of background segmentation; even for a less accurate algorithm such as MOG.

Moving to the MEU, both reference FPGA implementations utilizing this module in a single core. The parameter estimation phase takes from several seconds to up to a couple of minutes for the FPGA and same applies for the ARM A9. As this process is performed only once upon initialization of the system it is not a limiting factor for the applicability of the scheme and for this reason we are not focusing on accelerating further this module. In very low-end devices it could be omitted at all and the model parameters could be computed and sent from the outside (e.g., from an embedded CPU).

VIII. CONCLUSIONS

In this work a novel algorithm for background subtraction was presented which is suitable for in-camera acceleration in thermal imagery. The presented scheme through an automated parameter estimation process, takes into account the special characteristics of data, and gives highly accurate results without any fine-tuning from the user. It is implemented in reconfigurable hardware using a HLS design flow with no approximations in accuracy, arithmetic or in the mathematical formulation of the proposed algorithm. Unlike previously introduced custom-fit hardware accelerators, our scheme is platform independent, scalable and easily maintainable. Finally, to the best of our knowledge this is the first time that the very demanding task of background subtraction can be executed to thermal camera sensor in real-time and at low power budget, which allows for a distributed new approach that avoids the bottlenecks of the existing centralized solutions.

APPENDIX A

DERIVATION OF OPTIMAL VARIATIONAL DISTRIBUTIONS

Using (8) and (9) the logarithm of $q^*(\mathbf{Z})$ is given by

$$\ln q^*(\mathbf{Z}) = \mathbb{E}_{\varpi}[\ln p(\mathbf{Z}|\varpi)] + \mathbb{E}_{\mu, \tau}[\ln p(\mathbf{X}|\mathbf{Z}, \mu, \tau)] + \mathcal{C} \quad (34)$$

substituting (5) and (6) into (34) we get

$$\ln q^*(\mathbf{Z}) = \sum_{n=1}^N \sum_{k=1}^K z_{nk} \left(\mathbb{E}[\ln \varpi_k] + \frac{1}{2} \mathbb{E}[\ln \tau_k] - \frac{1}{2} \ln 2\pi - \frac{1}{2} \mathbb{E}_{\mu, \tau}[(x_n - \mu_k)^2 \tau_k] \right) + \mathcal{C} \Rightarrow$$

Using (9) and (8) the logarithm of $q^*(\varpi, \mu, \tau)$ is

$$\begin{aligned} \ln q^*(\varpi, \mu, \tau) &= \mathbb{E}_{\mathbf{Z}} [\ln p(\mathbf{X}|\mathbf{Z}, \mu, \tau) + \\ &+ \ln p(\mathbf{Z}|\varpi) + \\ &+ \ln p(\varpi) + \ln p(\mu, \tau)] + \mathcal{C} = \end{aligned} \quad (36a)$$

$$\begin{aligned} &= \sum_{n=1}^N \sum_{k=1}^K \mathbb{E}[z_{nk}] \ln \mathcal{N}(x_n | \mu_k, \tau_k^{-1}) + \\ &+ \mathbb{E}_{\mathbf{Z}} [\ln p(\mathbf{Z}|\varpi)] \\ &+ \ln p(\varpi) + \sum_{k=1}^K \ln p(\mu_k, \tau_k) + \mathcal{C} \end{aligned} \quad (36b)$$

Due to the fact that there is no term in (36b) that contains parameters from both sets $\{\varpi\}$ and $\{\mu, \tau\}$, the distribution $q^*(\varpi, \mu, \tau)$ can be factorized as $q(\varpi, \mu, \tau) = q(\varpi) \prod_{k=1}^K q(\mu_k, \tau_k)$. The distribution for $q^*(\varpi)$ is derived using only those terms of (36b) that depend on the variable ϖ . Therefore the logarithm of $q(\varpi)$ is given by

$$\ln q^*(\varpi) = \mathbb{E}_{\mathbf{Z}} [\ln p(\mathbf{Z}|\varpi)] + \ln p(\varpi) + \mathcal{C} = \quad (37a)$$

$$= \sum_{k=1}^K \ln \varpi_k^{(\sum_{n=1}^N r_{nk} + \lambda_0 - 1)} + \mathcal{C} = \quad (37b)$$

$$= \sum_{k=1}^K \ln \varpi_k^{(N_k + \lambda_0 - 1)} + \mathcal{C} \quad (37c)$$

We have made use of $\mathbb{E}[z_{nk}] = r_{nk}$, and we have denote as $N_k = \sum_{n=1}^N r_{nk}$. (37c) suggests that $q^*(\varpi)$ is a Dirichlet distribution with hyperparameters $\lambda = \{N_k + \lambda_0\}_{k=1}^K$.

Using only those terms of (36b) that depend on variables μ and τ , the logarithm of $q^*(\mu_k, \tau_k)$ is given by

$$\begin{aligned} \ln q^*(\mu_k, \tau_k) &= \ln \mathcal{N}(\mu_k | m_0, (\beta_0 \tau_k)^{-1}) + \\ &+ \ln \text{Gam}(\tau_k | a_0, b_0) + \\ &+ \sum_{n=1}^N \mathbb{E}[z_{nk}] \ln \mathcal{N}(x_n | \mu_k, \tau_k^{-1}) + \mathcal{C} = \\ &= -\frac{\beta_0 \tau_k}{2} (\mu_k - m_0)^2 + \frac{1}{2} \ln(\beta_0 \tau_k) + \\ &+ (a_0 - 1) \ln \tau_k - b_0 \tau_k - \\ &- \frac{1}{2} \sum_{n=1}^N \mathbb{E}[z_{nk}] (x_n - \mu_k)^2 \tau_k + \\ &+ \frac{1}{2} \left(\sum_{n=1}^N \mathbb{E}[z_{nk}] \right) \ln(\beta_0 \tau_k) + \mathcal{C} \end{aligned} \quad (38)$$

For the estimation of $q^*(\mu_k | \tau_k)$, we use (38) and keep only

those factors that depend on μ_k .

$$\begin{aligned} \ln q^*(\mu_k | \tau_k) &= -\frac{\beta_0 \tau_k}{2} (\mu_k - m_0)^2 - \\ &- \frac{1}{2} \sum_{n=1}^N \mathbb{E}[z_{nk}] (x_n - \mu_k)^2 \tau_k = \end{aligned} \quad (39a)$$

$$\begin{aligned} &= -\frac{1}{2} \mu_k^2 (\beta_0 + N_k) \tau_k + \\ &+ \mu_k \tau_k (\beta_0 m_0 + N_k \bar{x}_k) + \mathcal{C} \Rightarrow \end{aligned} \quad (39b)$$

$$q^*(\mu_k | \tau_k) = \mathcal{N}(\mu_k | m_k, (\beta_k \tau_k)^{-1}) \quad (39c)$$

where $\bar{x}_k = \frac{1}{N_k} \sum_{n=1}^N r_{nk} x_n$, $\beta_k = \beta_0 + N_k$ and $m_k = \frac{1}{\beta_k} (\beta_0 m_0 + N_k \bar{x}_k)$.

After the estimation of $q^*(\mu_k | \tau_k)$, logarithm of the optimized distribution $q^*(\tau_k)$ is given by

$$\ln q^*(\tau_k) = \ln q^*(\mu_k, \tau_k) - \ln q^*(\mu_k | \tau_k) = \quad (40a)$$

$$\begin{aligned} &= \left(a_0 + \frac{N_k}{2} - 1 \right) \ln \tau_k - \\ &- \frac{1}{2} \tau_k \left(\beta_0 (\mu_k - m_0)^2 + \right. \end{aligned} \quad (40b)$$

$$\begin{aligned} &+ 2b_0 + \sum_{n=1}^N r_{nk} (x_n - \mu_k)^2 - \\ &- \beta_k (\mu_k - m_k)^2 \left. \right) + \mathcal{C} \Rightarrow \end{aligned} \quad (40b)$$

$$q^*(\tau_k) = \text{Gam}(\tau_k | a_k, b_k) \quad (40c)$$

The parameters a_k and b_k are given by

$$a_k = a_0 + \frac{N_k}{2} \quad (41a)$$

$$b_k = b_0 + \frac{1}{2} \left(N_k \sigma_k + \frac{\beta_0 N_k}{\beta_0 + N_k} (\bar{x}_k - m_0)^2 \right) \quad (41b)$$

where $\sigma_k = \frac{1}{N_k} \sum_{n=1}^N (x_n - \bar{x}_k)^2$.

REFERENCES

- [1] R. Gade, A. Jorgensen, and T. Moeslund, "Long-term occupancy analysis using graph-based optimisation in thermal imagery," in *2013 IEEE Conference on Computer Vision and Pattern Recognition (CVPR)*, Jun. 2013, pp. 3698–3705.
- [2] W. Wang, J. Zhang, and C. Shen, "Improved human detection and classification in thermal images," in *2010 17th IEEE International Conference on Image Processing (ICIP)*, Sep. 2010, pp. 2313–2316.
- [3] J. W. Davis and V. Sharma, "Robust background-subtraction for person detection in thermal imagery," in *Proceedings of the 2004 Conference on Computer Vision and Pattern Recognition Workshop (CVPRW'04) Volume 8 - Volume 08*, ser. CVPRW '04. Washington, DC, USA: IEEE Computer Society, 2004, pp. 128–.
- [4] Q.-C. Pham, L. Gond, J. Begard, N. Alleazard, and P. Sayd, "Real-time posture analysis in a crowd using thermal imaging," in *Computer Vision and Pattern Recognition, 2007. CVPR'07. IEEE Conference on.* IEEE, 2007, pp. 1–8.
- [5] S.-C. S. Cheung and C. Kamath, "Robust background subtraction with foreground validation for urban traffic video," *EURASIP Journal on Advances in Signal Processing*, vol. 2005, no. 14, p. 726261, Aug. 2005.
- [6] F. Porikli, "Achieving real-time object detection and tracking under extreme conditions," *Journal of Real-Time Image Processing*, vol. 1, no. 1, pp. 33–40, Mar. 2006.
- [7] O. Tuzel, F. Porikli, and P. Meer, "Human detection via classification on riemannian manifolds," in *IEEE Conference on Computer Vision and Pattern Recognition, 2007. CVPR '07*, Jun. 2007, pp. 1–8.

- [8] —, “Pedestrian detection via classification on riemannian manifolds,” *IEEE Transactions on Pattern Analysis and Machine Intelligence*, vol. 30, no. 10, pp. 1713–1727, Oct. 2008.
- [9] K. Jungling and M. Arens, “Feature based person detection beyond the visible spectrum,” in *IEEE Computer Society Conference on Computer Vision and Pattern Recognition Workshops, 2009. CVPR Workshops 2009*, Jun. 2009, pp. 30–37.
- [10] L. Latecki, R. Miezianko, and D. Pokrajac, “Tracking motion objects in infrared videos,” in *IEEE Conference on Advanced Video and Signal Based Surveillance, 2005. AVSS 2005*, Sep. 2005, pp. 99–104.
- [11] M. J. Wainwright and M. I. Jordan, “Graphical models, exponential families, and variational inference,” *Foundations and Trends® in Machine Learning*, vol. 1, no. 1–2, pp. 1–305, 2008.
- [12] S. Brutzer, B. Hoferlin, and G. Heidemann, “Evaluation of background subtraction techniques for video surveillance,” in *2011 IEEE Conference on Computer Vision and Pattern Recognition (CVPR)*, Jun. 2011, pp. 1937–1944.
- [13] S. Herrero and J. Bescs, “Background subtraction techniques: Systematic evaluation and comparative analysis,” in *Proceedings of the 11th International Conference on Advanced Concepts for Intelligent Vision Systems*, ser. ACIVS '09. Berlin, Heidelberg: Springer-Verlag, 2009, pp. 33–42.
- [14] F. El Baf, T. Bouwmans, and B. Vachon, “Fuzzy statistical modeling of dynamic backgrounds for moving object detection in infrared videos,” in *IEEE Computer Society Conference on Computer Vision and Pattern Recognition Workshops, 2009. CVPR Workshops 2009*, Jun. 2009, pp. 60–65.
- [15] N. J. B. McFarlane and C. P. Schofield, “Segmentation and tracking of piglets in images,” *Machine Vision and Applications*, vol. 8, no. 3, pp. 187–193, May 1995.
- [16] J. Zheng, Y. Wang, N. Nihan, and M. Hallenbeck, “Extracting roadway background image: Mode-based approach,” *Transportation Research Record: Journal of the Transportation Research Board*, vol. 1944, pp. 82–88, Jan. 2006.
- [17] A. Elgammal, D. Harwood, and L. Davis, “Non-parametric model for background subtraction,” in *Computer Vision ECCV 2000*, ser. Lecture Notes in Computer Science, D. Vernon, Ed. Springer Berlin Heidelberg, Jan. 2000, no. 1843, pp. 751–767.
- [18] C. Wren, A. Azarbayejani, T. Darrell, and A. Pentland, “Pfinder: real-time tracking of the human body,” *IEEE Transactions on Pattern Analysis and Machine Intelligence*, vol. 19, no. 7, pp. 780–785, Jul. 1997.
- [19] S. Messelodi, C. M. Modena, N. Segata, and M. Zanin, “A kalman filter based background updating algorithm robust to sharp illumination changes,” in *Image Analysis and Processing ICIAP 2005*, ser. Lecture Notes in Computer Science, F. Roli and S. Vitulano, Eds. Springer Berlin Heidelberg, Jan. 2005, no. 3617, pp. 163–170.
- [20] K. Toyama, J. Krumm, B. Brumitt, and B. Meyers, “Wallflower: principles and practice of background maintenance,” in *The Proceedings of the Seventh IEEE International Conference on Computer Vision, 1999*, vol. 1, 1999, pp. 255–261 vol.1.
- [21] C. Stauffer and W. Grimson, “Adaptive background mixture models for real-time tracking,” in *Computer Vision and Pattern Recognition, 1999. IEEE Computer Society Conference on.*, vol. 2, 1999, pp. –252 Vol. 2.
- [22] K. Makantasis, A. Doulamis, and N. Matsatsinis, “Student-t background modeling for persons’ fall detection through visual cues,” in *2012 13th International Workshop on Image Analysis for Multimedia Interactive Services (WIAMIS)*, May 2012, pp. 1–4.
- [23] Z. Zivkovic, “Improved adaptive gaussian mixture model for background subtraction,” in *Proceedings of the 17th International Conference on Pattern Recognition, 2004. ICPR 2004*, vol. 2, Aug. 2004, pp. 28–31 Vol.2.
- [24] Z. Zivkovic and F. van der Heijden, “Efficient adaptive density estimation per image pixel for the task of background subtraction,” *Pattern Recognition Letters*, vol. 27, no. 7, pp. 773–780, May 2006.
- [25] T. Haines and T. Xiang, “Background subtraction with DirichletProcess mixture models,” *IEEE Transactions on Pattern Analysis and Machine Intelligence*, vol. 36, no. 4, pp. 670–683, Apr. 2014.
- [26] J. Davis and V. Sharma, “Fusion-based background-subtraction using contour saliency,” in *IEEE Computer Society Conference on Computer Vision and Pattern Recognition - Workshops, 2005. CVPR Workshops*, Jun. 2005, pp. 11–11.
- [27] J. W. Davis and V. Sharma, “Background-subtraction in thermal imagery using contour saliency,” *International Journal of Computer Vision*, vol. 71, no. 2, pp. 161–181, Feb. 2007.
- [28] T. Elguebaly and N. Bouguila, “Finite asymmetric generalized gaussian mixture models learning for infrared object detection,” *Computer Vision and Image Understanding*, vol. 117, no. 12, pp. 1659–1671, Dec. 2013.
- [29] C. Dai, Y. Zheng, and X. Li, “Pedestrian detection and tracking in infrared imagery using shape and appearance,” *Computer Vision and Image Understanding*, vol. 106, no. 23, pp. 288–299, May 2007.
- [30] P. Carr, “Gpu accelerated multimodal background subtraction,” in *Digital Image Computing: Techniques and Applications*. IEEE, 2008, pp. 279–286.
- [31] V. Pham, P. Vo, V. T. Hung *et al.*, “Gpu implementation of extended gaussian mixture model for background subtraction,” in *Computing and Communication Technologies, Research, Innovation, and Vision for the Future (RIVF), 2010 IEEE RIVF International Conference on*. IEEE, 2010, pp. 1–4.
- [32] C. Zhang, H. Tabkhi, and G. Schirner, “A gpu-based algorithm-specific optimization for high-performance background subtraction,” in *Parallel Processing (ICPP), 2014 43rd International Conference on*. IEEE, 2014, pp. 182–191.
- [33] F. Kristensen, H. Hedberg, H. Jiang, P. Nilsson, and V. Öwall, “An embedded real-time surveillance system: Implementation and evaluation,” *Journal of Signal Processing Systems*, vol. 52, no. 1, pp. 75–94, 2008.
- [34] H. Jiang, H. Ardö, and V. Öwall, “A hardware architecture for real-time video segmentation utilizing memory reduction techniques,” *Circuits and Systems for Video Technology, IEEE Transactions on*, vol. 19, no. 2, pp. 226–236, 2009.
- [35] M. Genovese and E. Napoli, “Fpga-based architecture for real time segmentation and denoising of hd video,” *Journal of Real-Time Image Processing*, vol. 8, no. 4, pp. 389–401, 2013.
- [36] —, “Asic and fpga implementation of the gaussian mixture model algorithm for real-time segmentation of high definition video,” *Very Large Scale Integration (VLSI) Systems, IEEE Transactions on*, vol. 22, no. 3, pp. 537–547, 2014.
- [37] C. Bishop, *Pattern Recognition and Machine Learning (Information Science and Statistics)*. Springer, Oct. 2007.
- [38] P. Diaconis, D. Ylvisaker *et al.*, “Conjugate priors for exponential families,” *The Annals of statistics*, vol. 7, no. 2, pp. 269–281, 1979.
- [39] D. Fink, “A compendium of conjugate priors,” See <http://www.people.cornell.edu/pages/df36/CONJINTRnew%20TEX.pdf>, p. 46, 1997.
- [40] S. Boyd and L. Vandenberghe, *Convex Optimization*. Cambridge University Press, Mar. 2004.
- [41] D. Arthur and S. Vassilvitskii, “k-means++: The advantages of careful seeding,” in *Proceedings of the eighteenth annual ACM-SIAM symposium on Discrete algorithms*. Society for Industrial and Applied Mathematics, 2007, pp. 1027–1035.
- [42] R. Yang and J. O. Berger, *A catalog of noninformative priors*. Institute of Statistics and Decision Sciences, Duke University, 1996.
- [43] S. Dasgupta and D. Hsu, “On-line estimation with the multivariate gaussian distribution,” in *Proceedings of the 20th Annual Conference on Learning Theory*, ser. COLT’07. Berlin, Heidelberg: Springer-Verlag, 2007, pp. 278–292.
- [44] Y. Shen, W. Hu, J. Liu, M. Yang, B. Wei, and C. T. Chou, “Efficient background subtraction for real-time tracking in embedded camera networks,” in *Proceedings of the 10th ACM Conference on Embedded Network Sensor Systems*. ACM, 2012, pp. 295–308.